ENERGY LABORATORY

MASSACHUSETTS INSTITUTE
OF TECHNOLOGY

INTERFACIAL EXCHANGE RELATIONS FOR TWO-FLUID VAPOR-LIQUID FLOW A SIMPLIFIED REGIME MAP APPROACH

by

J. E. Kelly and M. S. Kazimi

MIT Energy Laboratory Electric Utility Program
Report No. MIT-EL-81-024

May 1981

Energy Laboratory
and
Department of Nuclear Engineering

Massachusetts Institute of Technology
Cambridge, Mass. 02139

INTERFACIAL EXCHANGE RELATIONS FOR TWO-FLUID VAPOR-LIQUID FLOW A SIMPLIFIED REGIME MAP APPROACH

by

J. E. Kelly and M. S. Kazimi

May 1981

Sponsored by

Boston Edison Company
Northeast Utilities Service Company
Public Service Electric and Gas Company
Yankee Atomic Electric Company

under

MIT Energy Laboratory Electric Utility Program
Report No. MIT-EL-81-024

REPORTS IN REACTOR THERMAL HYDRAULICS RELATED TO THE MIT ENERGY LABORATORY ELECTRIC POWER PROGRAM

A. Topical Reports (For availability check Energy Laboratory Headquarters, Headquarters, Room E19-439, MIT, Cambridge, Massachusetts 02139)

A.1 General Applications
A.2 PWR Applications
A.3 BWR Applications
A.4 LMFBR Applications

A.1 J.E. Kelly, J. Loomis, L. Wolf, "LWR Core Thermal-Hydraulic Analysis--Assessment and Comparison of the Range of Applicability of the Codes COBRA-IIIC/MIT and COBRA-IV-1," MIT Energy Laboratory Report No. MIT-EL-78-026, September 1978.

M.S. Kazimi and M. Massoud, "A Condensed Review of Nuclear Reactor Thermal-Hydraulic Computer Codes for Two-Phase Flow Analysis," MIT Energy Energy Laboratory Report No. MIT-EL-79-018, February 1979.

J.E. Kelly and M.S. Kazimi, "Development and Testing of the Three Dimensional, Two-Fluid Code THERMIT for LWR Core and Subchannel Applications," MIT Energy Laboratory Report No. MIT-EL-79-046.

J.N. Loomis and W.D. Hinkle, "Reactor Core Thermal-Hydraulic Analysis--Improvement and Application of the Code COBRA-IIIC/MIT," MIT Energy Laboratory Report No. MIT-EL-80-027, September 1980.

D.P. Griggs, A.F. Henry and M.S. Kazimi, "Development of a Three-Dimensional Two-Fluid Code with Transient Neutronic Feedback for LWR Applications," MIT Energy Laboratory No. MIT-EL-81-013, April 1981.

J.E. Kelly, S.P. Kao and M.S. Kazimi, "THERMIT-2: A Two-Fluid Model for Light Water Reactor Subchannel Transient Analysis," MIT Energy Laboratory Report No. MIT-EL-81-014, April 1981.

A.2 P. Moreno, C. Chiu, R. Bowring, E. Khan, J. Liu, and N. Todreas, "Methods for Steady-State Thermal/Hydraulic Analysis of PWR Cores," MIT Energy Laboratory Report No. MIT-EL-76-006, Rev. 1, July 1977 (Orig. 3/77).

J. Liu, and N. Todreas, "Transient Thermal Analysis of PWR's by a Single Pass Procedure Using a Simplified Model Layout," MIT Energy Laboratory Report MIT-EL-77-008, Final, February 1979, (Draft, June 1977).

J. Liu, and N. Todreas, "The Comparison of Available Data on PWR Assembly Thermal Behavior with Analytic Predictions," MIT Energy Laboratory Report MIT-EL-77-009, Final, February 1979, (Draft, June 1977).

A.3 L. Guillebaud, A. Levin, W. Boyd, A. Faya, and L. Wolf, "WOSUB-A Subchannel Code for Steady-State and Transient Thermal-Hydraulic Analysis of Boiling Water Reactor Fuel Bundles," Vol. II, Users Manual, MIT-EL-78-024, July 1977.

L. Wolf, A. Faya, A. Levin, W. Boyd, L. Guillebaud, "WOSUB-A Subchannel Code for Steady-State and Transient Thermal-Hydraulic Analysis of Boiling Water Reactor Fuel Pin Bundles," Vol. III, Assessment and Comparison, MIT-EL-78-025, October 1977.

L. Wolf, A. Faya, A. Levin, L. Guillebaud, "WOSUB-A Subchannel Code for Steady-State Reactor Fuel Pin Bundles," Vol. I, Model Description, MIT-EL-78-023, September 1978.

A. Faya, L. Wolf and N. Todreas, "Development of a Method for BWR Subchannel Analysis," MIT-EL-79-027, November 1979.

A. Faya, L. Wolf and N. Todreas, "CANAL User's Manual," MIT-EL-79-028, November 1979.

A.4 W.D. Hinkle, "Water Tests for Determining Post-Voiding Behavior in the LMFBR," MIT Energy Laboratory Report MIT-EL-76-005, June 1976.

W.D. Hinkle, Ed., "LMFBR Safety and Sodium Boiling - A State of the Art Report," Draft DOE Report, June 1978.

M.R. Granziera, P. Griffith, W.D. Hinkle, M.S. Kazimi, A. Levin, M. Manahan, A. Schor, N. Todreas, G. Wilson, "Development of Computer Code for Multi-dimensional Analysis of Sodium Voiding in the LMFBR," Preliminary Draft Report, July 1979.

M. Granziera, P. Griffith, W. Hinkle (ed.), M. Kazimi, A. Levin, M. Manahan, A. Schor, N. Todreas, R. Vilim, G. Wilson, "Development of Computer Code Models for Analysis of Subassembly Voiding in the LMFBR," Interim Report of the MIT Sodium Boiling Project Covering Work Through September 30, 1979, MIT-EL-80-005.

A. Levin and P. Griffith, "Development of a Model to Predict Flow Oscillations in Low-Flow Sodium Boiling," MIT-EL-80-006, April 1980.

M.R. Granziera and M. Kazimi, "A Two-Dimensional, Two-Fluid Model for Sodium Boiling in LMFBR Assemblies," MIT-EL-80-011, May 1980.

G. Wilson and M. Kazimi, "Development of Models for the Sodium Version of the Two-Phase Three Dimensional Thermal Hydraulics Code THERMIT," MIT-EL-80-010, May 1980.

B. Papers

B.1 General Applications
B.2 PWR Applications
B.3 BWR Applications
B.4 LMFBR Application

B.1 J.E. Kelly and M.S. Kazimi, "Development of the Two-Fluid Multi-Dimensional Code THERMIT for LWR Analysis," Heat Transfer-Orlando 1980, AIChE Symposium Series 199, Vol. 76, August 1980.

J.E. Kelly and M.S. Kazimi, "THERMIT, A Three-Dimensional, Two-Fluid Code for LWR Transient Analysis," Transactions of American Nuclear Society, 34, p. 893, June 1980.

B.2 P. Moreno, J. Kiu, E. Khan, N. Todreas, "Steady State Thermal Analysis of PWR's by a Single Pass Procedure Using a Simplified Method," American Nuclear Society Transactions, Vol. 26.

P. Moreno, J. Liu, E. Khan, N. Todreas, "Steady-State Thermal Analysis of PWR's by a Single Pass Procedure Using a Simplified Nodal Layout," Nuclear Engineering and Design, Vol. 47, 1978, pp. 35-48.

C. Chiu, P. Moreno, R. Bowring, N. Todreas, "Enthalpy Transfer between PWR Fuel Assemblies in Analysis by the Lumped Subchannel Model," Nuclear Engineering and Design, Vol. 53, 1979, 165-186.

B.3 L. Wolf and A. Faya, "A BWR Subchannel Code with Drift Flux and Vapor Diffusion Transport," American Nuclear Society Transactions, Vol. 28, 1978, p. 553.

S.P. Kao and M.S. Kazimi, "CHF Predictions In Rod Bundles," Trans. ANS, 35, 766 June 1981.

B.4 W.D. Hinkle, (MIT), P.M. Tschamper (GE), M.H. Fontana (ORNL), R.E. Henry (ANL), and A. Padilla (HEDL), for U.S. Department of Energy, "LMFBR Safety & Sodium Boiling," paper presented at the ENS/ANS International Topical Meeting on Nuclear Reactor Safety, October 16-19, 1978, Brussels, Belgium.

M.I. Autruffe, G.J. Wilson, B. Stewart and M. Kazimi, "A Proposed Momentum Exchange Coefficient for Two-Phase Modeling of Sodium Boiling," Proc. Int. Meeting Fast Reactor Safety Technology, Vol. 4, 2512-2521, Seattle, Washington, August 1979.

M.R. Granziera and M.S. Kazimi, "NATOF-2D: A Two Dimensional Two-Fluid Model for Sodium Flow Transient Analysis," Trans. ANS, 33, 515, November 1979.

Interfacial Exchange Relations for Two-Fluid Vapor-Liquid Flow: A Simplified Regime Map Approach

Abstract

A simplified approach is described for selection of the constitutive relations for the inter-phase exchange terms in the two-fluid code, THERMIT. The approach used distinguishes between pre-CHF and post-CHF conditions. Interfacial mass, energy and momentum exchange terms are selected and tested against one dimensional measurements for a wide range of mass flow rate, pressure and void fraction conditions. It is concluded that the simplified regime map approach leads to accurate predictions for LWR applications, excluding depressurization events.

NOMENCLATURE

A_i	Interfacial Area
C_d	Drag Coefficient
C_i	Interfacial Momentum Exchange Coefficient
C_p	Specific Heat
D	Diameter
F_i	Vapor-Liquid Interfacial Momentum Exchange Rate
g	Gravitational Constant
G	Mass Flux
H	Heat Transfer Coefficient
i	Enthalpy
k	Thermal Conductivity
P	Pressure
Pr	Prandtl Number
Q_i	Interfacial Heat Transfer Rate
Q_W	Wall Heat Transfer Rate
$\dot{q}$	Power
q"	Heat Flux
R_b	Bubble Radius
Re	Reynolds Number
S	Slip Ratio (V_v/V_ℓ)
t	Time
T	Temperature
T_d	Bubble Departure Temperature
V	Velocity

Nomenclature (continued)

V_r	Relative Velocity ($V_v - V_\ell$)
We	Weber Number
X	Quality
α	Void Fraction
σ	Surface Tension
Γ	Vapor Generation Rate
ρ	Density
μ	Viscosity
τ	Shear Force
δ	Droplet Diameter

Subscripts

c	Continuous Phase
d	Droplet
e	Equilibrium
f	Saturated Liquid
g	Saturated Vapor
i	Interfacial
ℓ	Liquid
s	Saturation
v	Vapor
w	Wall
cr	Critical Point

Introduction

The physical phenomena encountered during transient two-phase coolant flow in nuclear reactors have been shown by several authors to require modeling of the liquid and vapor as separate but coupled flow fields. The coupling of the flow fields is done through interfacial exchange terms for mass, energy and momentum. This two-fluid approach to the flow representation has the advantage of allowing flexibility for unequal temperatures and unequal velocities of the two phases, as well as bidirectional flow of vapor and liquid. Unfortunately, the mathematical formulation of the exchange terms is complicated by the microscopic nature of the transfer processes. In fact, precise modeling of these processes on a local basis is virtually impossible.

From a practical point of view, what must be modeled is usually the net effect of all microscopic transfers within a finite control volume. This task is easier, although it introduces certain arbitrariness [1]. Increasingly, a number of investigators argue for the need to improve the accuracy and/or the numerical efficiency of the two-fluid calculations by introducing coupling terms that reflect the details of the microscopic nature of the transfer processes. This approach leads directly to a complicated choice of constitutive relations that rely heavily on a priori determination of several flow regimes [1,2].

The complexity of the search for constitutive relations is sometimes shown not to affect the physical results but improve the numerical efficiency [3]. For a wide range of transient applications, it may be more efficient to simplify the search for the constitutive equations, by selecting the interaction terms to apply over a spectrum of flow regimes.

In this paper it will be shown that through relatively straightforward but careful consideration of the physical phenomena appropriate macroscopic exchange terms can be formulated for applications over a wide range of conditions. This allows a simple flow map to be used. The interfacial exchange models described here have been incorporated in the computer code THERMIT [4,5], which is based on a two-fluid model for two-phase flow (see Table 1 for equations). These models were then assessed and improved using experimental measurements available in the open literature. The measurements used in the assessment of these models were typical of LWR operating conditions. Consequently, the models described here should be applicable for conditions of practical importance in LWR operation and safety.

However, other two-fluid models in computer codes such as TRAC-PIA [6] and UVUT [7] use elaborate flow regime maps to determine the appropriate interfacial exchange models for a given set of flow conditions. The interfacial exchange models in TRAC have recently been reviewed by Rohatgi and Saha [8], and the vessel module interfacial exchange models are summarized in Table 2. The complexity introduced by using a flow regime map is evident by the large number of constitutive relations which are needed. As will be shown in this paper, a simpler approach to the flow regime dependence of the interfacial exchange models reduces the number of required constitutive equations (and associated logic) while maintaining good representation of the available data.

Interfacial Mass Exchange

Background

The exchange of mass across liquid-vapor interfaces must be explicitly modeled in the two-fluid model. In reactor applications, this exchange usually takes the form of vapor generation so that the mass exchange model is also referred to as the vapor generation model. This exchange of mass is strongly dependent on the flow conditions and for BWR conditions at least three different vaporization regimes can be identified (Flashing is not considered in this model). The first, termed subcooled boiling, occurs even though the bulk liquid is subcooled provided the heat flux is high enough to allow vapor bubbles to grow and detach from the heater surface. However, since the liquid is subcooled, condensation of the vapor in the bulk fluid may also occur. Consequently, for subcooled boiling conditions, both vaporization and condensation need to be modeled.

The second vaporization regime, termed saturated boiling, occurs when the bulk liquid is at saturated conditions. For steady-state saturated conditions, all of the wall heat flux produces vapor (i.e., neither phase temperaure is increased). Hence, if the wall heat flux is known, the determination of the vapor generation rate follows from an energy balance.

The third type of vapor generation is that which occurs when a superheated vapor transfers heat to liquid droplets thus evaporating the droplets. This form of vaporization dominates after the critical heat flux (CHF) has been exceeded when the liquid can no longer wet the heater surface and, therefore, the entire wall heat flux is transferred directly to the vapor. Due to the relatively low conductivity of the vapor, a portion of the heat flux will superheat the vapor with the remainder vaporizing the liquid droplets.

By excluding depressurization transients, only these mechanisms need to be considered. Furthermore, the range of application of each vaporization mechanism can be defined according to the heat transfer regime. For pre-CHF conditions either subcooled or saturated boiling will occur. Hence, it is advantageous to describe both types of boiling in a single, continuous model so that the gradual transition from subcooled to saturated boiling is well represented. However, for post-CHF conditions a different vaporization model will be needed.

This approach of using the CHF condition to determine the appropriate vapor generation rate has been incorporated into THERMIT. The use of this simple selection scheme eliminates the need to have a more elaborate flow regime map.

Pre-CHF Vapor Generation Model Formulation

The pre-CHF vapor generation model in THERMIT accounts for both subcooled and saturated boiling. Since it is relatively easy to formulate a model to describe saturated boiling, the main difficulty lies in representing vapor generation for subcooled conditions.

On a microscopic scale, the subcooled vapor generation can be directly related to the vapor bubble rate of growth when the wall temperature exceeds the saturation temperature. Vapor bubbles are formed at nucleation sites on the heated surface and grow since superheated liquid exists near the wall. The bubbles remain attached until reaching a critical size which corresponds to a bulk liquid temperature equal to the bubble departure temperature, T_d. Once T_d has been exceeded the bubbles detach and flow into the main flow stream.

The value for T_d is found to be strongly dependent on the heat flux and flow conditions and has been correlated by many authors [9-11].

The correlation of Ahmad [9] has been selected for use in THERMIT. In this correlation, T_d is related to the heat flux through a heat transfer coefficient. The expressions for this relationship is given by

$$T_d = T_s - q''_w/H_A \tag{1}$$

The heat transfer coefficient H_A has been correlated using a large number of experimental measurements and is given by

$$H_A = \frac{k_\ell}{D}\left[2.44\ Re^{1/2}\ Pr^{1/3}\left(\frac{i_{in}}{i_f}\right)^{1/3}\left(\frac{i_{fg}}{i_f}\right)^{1/3}\right] \tag{2}$$

For a given set of flow conditions (i.e., H_A and T_s constant), if the heat flux is increased, T_d decreases as expected.

With T_d well defined by correlation, the vaporization rate based on bulk flow properties can be constructed using the following physical picture. For bulk liquid temperatures below T_d, bubbles do not detach and the net vaporization rate is zero. At the saturation limit, that is $T_\ell = T_s$, all of the wall heat flux leads directly to vapor generation so that the equilibrium vaporization rate, Γ_e, may be written as

$$\Gamma_e = \frac{\dot{q}_w}{i_{fg}} \tag{3}$$

where $\dot{q}_w$ is the power transferred to the coolant and i_{fg} is the heat of vaporization. If it is then assumed that the vaporization rate increases linearly from T_d to T_s the gross vapor generation rate, Γ_v, may be written as:

$$\Gamma_v = \begin{cases} 0 & \text{if } T_\ell < T_d \\ \dfrac{T_\ell - T_d}{T_s - T_d}\,\Gamma_e & \text{if } T_d \leq T_\ell < T_s \\ \Gamma_e & \text{if } T_\ell \geq \end{cases} \tag{4}$$

It is seen that this model correctly defaults to the saturated boiling model once the liquid becomes saturated. Although the assumption concerning the linear increase in Γ may not be strictly valid for all cases, it is seen as practically appropriate for most cases of interest.

If the bulk liquid is subcooled, the loss of vapor due to condensation must be accounted for. The model used to represent the condensation is relatively simple. The condensation rate, Γ_c, is modeled as a conduction-based term divided by the heat of vaporization. This can be written as:

$$\Gamma_c = A_i H_i (T_\ell - T_v)/i_{fg} \tag{5}$$

The term A_i represents the interfacial area per unit volume which for spherical bubbles of radius R_b may be written as

$$A_i = 3\alpha/R_b \tag{6}$$

where [9]:

$$R_b = \begin{cases} R_{bo} & \alpha < 0.1 \\ R_{bo}\left(\dfrac{9\alpha}{1-\alpha}\right)^{1/3} & \alpha \geq 0.1 \end{cases} \tag{7}$$

and

$$R_{bo} = 0.45 \sqrt{\frac{\sigma}{\rho_\ell - \rho_v}} \left[1 + 1.34((1-\alpha)V_\ell)^{1/3}\right]^{-1} \tag{8}$$

The interfacial heat transfer coefficient, H_i, is based on the effective conductivity of the two phases, and is given by

$$H_i = \begin{cases} \dfrac{k_\ell}{0.15R_{bo}} & T_v \leq T \quad \text{(evaporation)} \\ \dfrac{k_v k_\ell}{0.01R_{bo}\, k_\ell + 0.015R_{bo}\, k_v} & T_v > T \quad \text{(condensation)} \end{cases} \tag{9}$$

Both the vaporization and condensation terms can be combined to obtain the net vaporization rate:

$$\Gamma = \begin{cases} 0 & \text{if } T_\ell < T_d \\ \dfrac{T_\ell - T_d}{T_s - T_d}\, \Gamma_e + A_i H_i (T_\ell - T_v)/i_{fg} & \text{if } T_d < T_\ell < T_s \\ \Gamma_e & \text{if } T \geq T_s \end{cases} \tag{10}$$

Subcooled Vapor Generation Model-Assessment

From the previous discussion it is seen that this model is physically correct. The main characteristics of the model which have been assessed include the boiling incipient point and the vapor generation rate for subcooled conditions. Both of these characteristics have been assessed using steady-state, one-dimensional void fraction measurements. The boiling incipient point, which corresponds to the bubble departure temperature, can be clearly identified in the measurements which make the assessment of this characteristic rather straightforward.

The vapor generation rate in subcooled conditions can be directly related to the void fraction if the liquid and vapor velocities are nearly equal. This condition will be appropriate for void fractions at low quality and high pressure. For these cases the expression for the void fraction is

$$\alpha = \frac{1}{1 + \frac{1-X}{X} \frac{\rho_v}{\rho_\ell}} \tag{11}$$

The quality, in turn, can be related to the vapor generation rate via the vapor mass equation (simplified for one-dimensional, steady-state conditions):

$$\frac{\partial X}{\partial z} = \frac{\Gamma}{G} \tag{12}$$

Hence, the vapor generation rate is directly related to the void fraction and can be assessed with one-dimensional, steady-state void fraction measurements.

In the assessment effort, over 30 one-dimensional steady state void fraction comparison cases have been made. The data of Maurer [12], Marchaterre [13], and Christensen [14], have been used in this study. These data cover a wide range of flow conditions as seen in Table 3.

For assessing the vaporization rate, only comparisons at low qualities have been used. Excellent agreement has been found in these comparisons for both the boiling incipient point and the subcooled void fraction. Typical comparison cases, covering a range of pressures, are illustrated in Figures 1-3. The location where boiling begins is seen to be well predicted in each case. This good agreement indicates the appropriateness of Ahmad's correlation for the bubble departure temperature. The void fraction for subcooled conditions is also well predicted.

In view of the above comparisons and the inherent physical attributes of the subcooled vapor generation model, it can be stated that the model satisfactorily predicts subcooled boiling. Extending this model to three-dimensional cases also seems to be appropriate due to its mechanistic nature. Therefore, the subcooled vapor generation model should be applicable for all pre-CHF conditions except for depressurization transients (in which flashing becomes the significant vaporization mechanism).

It should be noted that the TRAC-P1A model cannot predict vaporization unless $T_\ell > T_s$. Thus, subcooled boiling cannot be modeled. However, the TRAC-P1A is capable of predicting vaporization during depressurization which leads to the fact that the primary application of TRAC-P1A would be LOCA analysis.

Post-CHF Vapor Generation-Formulation

After CHF has been exceeded the wall temperaure will rapidly increase and in a short period of time the minimum stable film boiling temperature,

T_{msfb}, will be exceeded. Once this temperature has been attained, the liquid can no longer wet the wall. Only by vapor-to-liquid heat transfer can the liquid be heated and evaporated. Hence, the rate of vapor generation is directly dependent on the rate of heat transfer from the vapor to the liquid. However, due to the low conductivity of the vapor, the vapor becomes superheated by a significant amount (e.g., 150 °K [15].

Once the correct heat transfer rate between phases is determined, the vaporization rate is found by simple dividing by the heat of vaporization:

$$\Gamma = A_i H_i (T_v - T_\ell)/i_{fg} \tag{13}$$

where A_i and H_i are the appropriate interfacial area and effective heat transfer coefficient. As discussed by Saha [16] each of these parameters may be written as a function of the flow variables, but ultimately a correlation is required to complete the function. To illustrate this point, the interfacial area per unit volume may be written as

$$A_i = \frac{6(1-\alpha)}{\delta} \tag{14}$$

where δ is the droplet diameter and the interfacial heat transfer coefficient can be correlated as a Nusselt number based on the droplet diameter:

$$H_i = \frac{k_v}{\delta}\left[2 + 0.459\left(\frac{\rho_v(V_v - V_\ell)\delta}{\mu_v}\right)^{0.55} Pr_v^{\ 0.33}\right] \tag{15}$$

However, δ needs to be determined from a correlation effectively causing both A_i and H_i to be correlated as functions of the flow conditions.

In view of this difficulty, Saha has combined the two parameters, A_i and H_i, into a single parameter K_1 which is then correlated as a function of the flow conditions. This approach eliminates the need to use two correlations which may be difficult to determine separately. The final form of this vaporization rate correlation is given by

$$\Gamma = 6300 \left[1 - \frac{P}{P_{cr}}\right]^2 \left[\frac{\rho_v V_v^2 D}{\sigma}\right]^{1/2} \frac{k_v (T_v - T_s)}{D^2 i_{fg}} (1 - \alpha) \qquad (16)$$

The droplet diameter has been assumed to be proportional to the hydraulic diameter, D. The interfacial area per unit volume is seen to be inversely proportional to D with the heat transfer coefficient being proportional to k_v/D. As the vapor velocity increases, the droplets become smaller, increasing the interfacial area and increasing Γ. Hence, this model apparently contains sufficient physical characteristics to predict the vaporization of liquid droplets.

Droplet Vaporization Model - Assessment

Obviously, the important quantity which this model is intended to predict is the rate of vapor generation for post-CHF conditions (or whenever vaporization of liquid droplets is significant). Unfortunately, this rate cannot be directly measured. Consequently, the assessment of the Saha model has required indirect methods. This assessment relies on the tight coupling between the degree of vapor superheat and the vaporization rate. When the total wall heat flux is known, an indirect assessment

of the vaporization rate can be made if the fraction of the heat flux which raises the vapor temperature can be determined.

This fraction is easily calculated if the vapor temperature is known. Unfortunately, the vapor temperature is not easily measured [15]. However, the vapor temperature can be inferred from wall temperature measurements using the known heat flux and an appropriate heat transfer coefficient. This method is straightforward provided the heat transfer coefficient is judiciously chosen. Since the heat transfer mechanism is primarily forced convection to the vapor, Saha recommends the use of a single-phase vapor forced convection heat transfer correlation.

Hence, wall temperature comparisons give a direct indication of the vapor temperature predictions which, in turn, relate to the vapor generation rate. Even though this procedure is indirect, it is the only viable method for assessing the post-CHF vapor generation rate, which is not measured directly.

For this study, the steady-state, one-dimensional wall temperature measurements of Bennett [17] have been used. A number of representative cases have been simulated. Comparison of measured and predicted post-CHF wall temperatures are in overall good agreement even though a range of conditions have been considered. Example comparisons are illustrated in Figures 4-6 for a range of mass velocities. It should be noted that the predicted CHF location has been adjusted to correspond with the measured value in order to accurately assess the post-CHF regime. In each case, the trend in the data is correctly predicted and good agreement is found except near the test section exit. These discrepancies are probably due to axial conduction effects which were not modeled in THERMIT.

Two other vapor generation models which represent limiting values are compared with the Saha model and measurements in Fig. 7. The first model, termed the equilibrium model, assumes that all of the wall heat flux leads to vapor production and may be written as

$$\Gamma = \frac{q_w}{i_{fg}} \tag{17}$$

When this model is used, the vapor does not superheat until all the liquid is evaporated and consequently the wall temperatures are underpredicted.

The second model, called the frozen quality model, assumes that Γ is zero after the CHF point which prevents the quality from changing. When this model is used, no evaporation is allowed so that all the wall heat is transferred to the vapor. Consequently, the vapor superheat as well as the wall temperatures are significantly overpredicted.

The comparisons with these two limiting models as well as with the data demonstrate the appropriateness of the Saha model for post-CHF vapor production. It may also be noted that the TRAC-P1A mass exchange model for annular mist flow closely resembles this model in form.

Interfacial Energy Exchange Formulation

The interfacial energy exchange rate represents the rate of energy transfer from one phase to the other. This transfer can be due to either conduction, which is a function of the temperature distribution, or mass transfer. If one considers the interface to be infinitesimally thin and at saturated conditions, then the energy transfer can be modeled. Defining the energy transfer as positive when the vapor receives the energy, the energy transfer rate may be written as:

$$Q_i = H_{i\ell} (T_\ell - T_s) + \Gamma i_f = H_{iv} (T_s - T_v) + \Gamma i_g \quad (18)$$

where $H_{i\ell}$ is the liquid-to-interface heat transfer coefficient and H_{iv} is the vapor-to-interface heat transfer coefficient. This equation shows that the rate of energy transfer from the liquid to the interface is the same as the energy transport rate from the interface into the vapor. In view of the equivalence of energy transfer rates, one may use either form.

In subcooled and saturated boiling conditions, or pre-CHF regime, the interface-to-vapor energy transfer can be appropriately modeled by considering the vapor to be at saturated conditions. In order to maintain the vapor at saturated conditions when the bulk liquid is subcooled, a relatively high rate of vapor-to-interface heat transfer is required which means that H_{iv} must be chosen sufficiently large, to maintain the vapor at saturation.

Consequently, for pre-CHF regime, the interfacial energy exchange is modeled as:

$$Q_i = H_{iv} (T_s - T_v) + \Gamma i_g \quad (19)$$

where H_{iv} is set to a very large value (10^{11} W/m^3) in order to force the vapor to be saturated. It should be noted that since the bulk liquid temperature is not used in this equation, the liquid temperature is unconstrained and may, therefore, be subcooled.

For post-CHF conditions, where droplet vaporization is the form of mass exchange, the superheated vapor is assumed to transfer heat by conduction to the interface while receiving energy due to the vaporization of the liquid. In this case, modeling of the vapor-to-interface energy

transfer is difficult unless the detailed vapor temperature distribution is known. However, the liquid-to-interface energy exchange can be adequately modeled since the liquid is assumed to be at or near saturation. Therefore, by simply choosing a value for $H_{i\ell}$ which is sufficiently large, the liquid will be forced to saturated conditions.

Consequently, for the post-CHF vaporization regime, the interfacial energy exchange is modeled as a liquid-to-interface energy transfer mechanism. This exchange rate may be written as

$$Q_i = \Gamma i_f - H_{i\ell} (T_s - T_\ell) \tag{20}$$

where $H_{i\ell}$ is set to a large value (10^{11} W/m^3) in order to force the liquid to saturation. The bulk vapor temperature is not constrained by this equation which allows the vapor to superheat. Hence, this model allows for the appropriate liquid and vapor temperatures to be predicted for the droplet vaporization regime.

Interfacial Energy Exchange Assessment

Validation of either of the preceeding approaches is difficult since the interfacial energy exchange cannot be directly related to a measureable quantity. Therefore, the models can only be assessed qualitatively by inference. For example, in subcooled conditions the bulk liquid temperature should be subcooled while the vapor should be saturated. Alternatively, for droplet vaporization, the vapor should be superheated with the liquid saturated. If these results are predicted, then the interfacial energy exchange rate is at least qualitatively correct.

These models have been used in all of the mass exchange rate validation studies and have yielded the expected results in all cases. A typical temperature profile is illustrated in Fig. 8. It is seen that the vapor temperature follows the saturation temperature which is decreasing due to the pressure drop. The liquid temperature is initially subcooled, but eventually reaches saturation near the end of the test section. Hence, for subcooled and saturated boiling conditions the interfacial energy exchange rate given by Eq. (19) seems to be an appropriate choice.

For post-CHF conditions similar results are obtained, as illustrated in Fig. 9. At the inlet, the liquid is subcooled but quickly becomes saturated and remains so along the entire heated length. The vapor remains at saturation before CHF, but quickly superheats after CHF has been attained. These predictions are the expected results so that the interfacial energy exchange model given by Eq. (20) seems to be an appropriate choice for post-CHF conditions.

The TRAC-P1A and THERMIT expressions cannot be compared directly due to the differences in formulation of conservation equations as well as the flow regime maps. However, it is seen that in THERMIT the interfacial heat transfer rate depends on the choice of interfacial mass exchange rate, Γ, while the reverse is true for the TRAC-P1A models.

It should also be noted that the choice of exchange model is again dictated by whether or not the CHF has been exceeded. The advantage of using this criterion is that it reduces the number of regimes to two. Also, this parameter is calculated as part of every analysis so that no additional calculation is required.

Interfacial Momentum Exchange - Formulation

The third type of interfacial exchange phenomena which must be modeled is the interfacial momentum exchange. This exchange controls the relative velocity of the two phases.

As in the case of the other interfacial exchange phenomena, the interfacial momentum exchange is strongly dependent on the flow conditions, since the structure of the two-phase flow changes with the flow conditions. In attempting to model the interfacial momentum exchange, it is necessary to consider the various forces which can act between the two phases. At least five different forces can be postulated to exist. These may be divided into steady flow and transient flow forces. The steady flow forces include viscous, inertial and buoyancy forces while the transient flow forces include the Bassett and virtual mass force [2,3]. The Bassett and virtual mass forces are significant only for rapidly accelerating flows and are not considered here. Also the buoyancy force should be small in comparison to the other forces and will not be considered. Hence only the viscous and inertial forces are retained in the THERMIT interfacial force model.

The viscous force, which arises due to the viscous shear stress is only significant at low relative velocities and can be approximately described by Stokes law. As discussed by Soo [18], modifications of Stokes law are required for systems in which the droplet (or sphere) is deformable (such as vapor bubbles in liquid). An example of such a modification is given by Levich [19].

$$F_{\mu} = 6\pi\mu_c D_d V_r \tag{21}$$

where V_r is the relative velocity, μ_c is the viscosity of the continuous phase and D_d is the equivalent diameter of the dispersed phase. This expression is similar to other expressions [18] and is valid for many practical droplet or bubble flow situations.

The force given by Eq. (21) represents the force on a single droplet and is converted to a force per unit volume, by dividing by the volume of a droplet and multiplying by the void fraction. Performing this operation yields

$$F_\mu = \frac{36\mu_c \alpha V_r}{D_d^2} \tag{22}$$

This expression represents the interfacial force due to viscous effects within a given control volume.

The second type of force is that due to inertial effects. This force, also referred to as the drag force, represents the momentum loss due to the motion of two continuous fluid streams relative to one another. Hence, this force tends to dominate in annular flow regimes. Following Wallis [20], the shear stress between the phases may be written as

$$\tau_i = 1/2 C_d \rho_v V_r^2 \tag{23}$$

Since the diameter of the vapor core is given by

$$D_c = D\sqrt{\alpha} \tag{24}$$

the interfacial force per unit volume is

$$F_i = \frac{2C_d \rho_v V_r^2 \sqrt{\alpha}}{D} \tag{25}$$

where C_d is the interfacial drag coefficient. Values for C_d, appropriate for annular flow, have been formulated with Wallis recommending the following value [20],

$$C_d = .005(1 + 75(1 - \alpha)) \tag{26}$$

Using this coefficient the interfacial drag force can be evaluated.

These two interfacial forces have been combined into a single expressions which is continuous for all flow regimes. Thus, no flow regime maps are required. However, the function form of the forces must be rearranged. Combining the two forces together, the interfacial exchange model in THERMIT is

$$F_i = \left(\frac{1 - \hat{\alpha}}{\hat{\alpha} D}\right)^2 \mu_\ell V_r + \left(\frac{1 - \hat{\alpha}}{\hat{\alpha} D}\right) \frac{\rho_v |V_r| V_r}{2} \tag{27}$$

where

$$\hat{\alpha} = \max(0.1, \alpha)$$

and

$$D = \text{hydraulic diameter}$$

$$V_r = V_v - V_\ell$$

The reason for the restriction on α is to prevent a singularity when $\alpha = 0$.

From the previous discussion, it should be obvious that the first term in this expression represents the viscous force while the second term represents the inertial drag force. Comparing the viscous term with Eq. (22), one finds that the following approximation has been made:

$$\frac{36\alpha}{D_v^2} \cong \left(\frac{1-\alpha}{\alpha D}\right)^2 \tag{28}$$

where D_v is the vapor bubble diameter appropriate for bubbly flow. Since this force is only significant in bubbly flow regime, the approximation here is only appropriate for low void fractions. This fact is illustrated in Table 4 where the two coefficients are compared for a range of void fractions assuming representative values for the diameters. For void fractions of approximately 0.15 and less, the approximated coefficient is comparable with the Levich model coefficient. However, this range corresponds to the conditions for which the viscous force is important.

The inertial force term in the interfacial momentum exchange model can be compared with Eq. (25). In order to equate the two expressions, the following approximation must be made.

$$2C_d \sqrt{\alpha} \cong \frac{1-\alpha}{2\alpha} \tag{29}$$

These two coefficients are compared in Table 5 over a range of void fractions. It is seen that at low void fractions the THERMIT model predicts a higher coefficient which is necessary to have continuity between the viscous and inertial regimes. However, at higher void fractions the two are approximately the same. Since annular flow would be expected for $\alpha > 0.6$, the approximated inertial drag coefficient in THERMIT seems

to be appropriate.

Hence, the formulation of the interfacial momentum exchange model seems to be satisfactory in spite of the approximations which have been made.

Interfacial Momentum Exchange - Assessment

The assessment of the interfacial momentum exchange model has employed the same one-dimensional void fraction measurements used to assess the interfacial mass transfer rate. While the verification of the mass exchange model was concerned with the low quality void fractions, assessment of the momentum exchange rate has relied on the high quality data. The reason for this is that only for thermal equilibrium conditions (i.e., non-subcooled conditions), can the momentum exchange rate be independently assessed with void fraction measurements. This fact can be illustrated by considering the definition of the void fraction:

$$\alpha = \frac{X}{X + (1 - X)\frac{\rho_v V_v}{\rho_\ell V_\ell}} \tag{30}$$

For a given pressure, the void fraction is seen to depend on the flow quality and the slip ratio, $S(S = V_v/V_\ell)$. The flow quality has been shown to depend on the vapor generation rate by Eq. (12) while the slip ratio depends on the interfacial force. For thermal equilibrium conditions the vaporization rate is known and the flow quality can be determined from an energy balance so that the momentum exchange rate can be assessed with void fraction measurements.

For assessing the interfacial momentum exchange rate, only the higher quality data have been used. Generally, the predictions agree rather well with the measured void fraction values over the range of flow conditions considered here. Typical comparison cases, covering a wide range of pressures, are illustrated in Figures 10-12. It is seen that in the higher quality regimes, the measured void fraction values are satisfactorily predicted in each case.

Again the TRAC-P1A and THERMIT relations can not be directly compared. It is seen, however, that what TRAC-P1A attempts to do on a flow regime basis, THERMIT does on a continuous basis. Due to the uncertainty in these terms as well as the good agreement with data which the THERMIT model exhibits it seems appropriate to use the simpler THERMIT expression.

Summary

The simplified approach to interfacial exchange expressions used in THERMIT have been described here and it is seen that the non-equilibrium phenomena are predicted in a realistic manner. These models are summarized in Table 6. It is quite apparent that compared to the TRAC-P1A modeling approach (Table 2), the THERMIT modeling approach is much simpler. Furthermore, it is not obvious that the more sophisticated approach produces more accurate results. In fact, the assessment work has shown that the simpler approach is indeed appropriate. Also, since the models are physically based, it is expected that they will be valid for regimes outside of their data base. This is an important point, since it justifies the use of these models for transients excluding depressurization.

REFERENCES

1. W. T. Hancox, R. L. Ferch, W. S. Liu and R. E. Neiman, "One-Dimensional Models for Transient Gas-Liquid Flows in Ducts," Int. J. Multiphase Flow, 25-40, 6, 1980.

2. M. Ishii and K. Mishima, "Two Fluid Model and Analysis for Interfacial Area," ANL/RAS/LWR80-3, Argonne National Laboratory, March 1980.

3. L. Y. Cheng, D. A. Drew, and R. T. Lahey, Jr., "Virtual Mass Effects in Two-Phase Flow," NUREG/CR-0020, (1978).

4. W. H. Reed and H. B. Stewart, "THERMIT: A Computer Program for Three-Dimensional Thermal-Hydraulic Analysis of Light Water Reactor Cores," M.I.T. Report prepared for EPRI, (1978).

5. J. E. Kelly, "Development of a Two-Fluid, Two-Phase Model for Light Water Reactor Subchannel Analysis," Ph.D. Thesis, Department of Nuclear Engineering, M.I.T., (1980).

6. "TRAC-P1A: An Advanced Best-Estimate Computer Program for PWR LOCA Analysis," LA-7777-MS, NUREG/CR-0665, Los Alamos National Laboratory (1979).

7. E. D. Hughes et al., "An Evaluation of State-of-the-Art Two-Velocity, Two-Phase Flow Models and Their Applicability to Nuclear Reactor Transient Analysis," NP-143, EPRI (1976).

8. U. S. Rohatgi and P. Saha, "Constitutive Relations in TRAC-P1A," NUREG/CR-1651, BNL-NUREG-51258, Brookhaven National Laboratory (1980).

9. S. Y. Ahmad, "Axial Distribution of Bulk Temperature anv Void Fraction in a Heated Channel with Inlet Subcooling," Journal of Heat Transfer, 92, p. 595, (1970).

10. P. Saha and N. Zuber, "Point of Net Vapor Generation and Vapor Void Fraction in Subcooled Boiling," Proceeding of the 5th International Heat Transfer Conference, (1974).

11. S. Levy, "Forced Convection Subcooled Boiling - Prediction of Vapor Volume Fraction," Int'l Journal of Heat and Mass Transfer, 10, p. 951, (1967).

12. G. W. Maurer, "A Method of Predicting Steady-State Boiling Vapor Fraction in Reactor Coolant Channels," WAPD-BT-19, (1960).

13. J. F. Marchaterre, et al., "Natural and Forced-Circulation Boiling Studies," ANL-5735, (1960).

References (continued)

14. H. Christensen, "Power-to-Void Transfer Functions," ANL-6385, (1961).

15. S. Nijhawan, et al., "Measurement of Vapor Superheat in Post-Critical Heat Flux Boiling," 18th National Heat Transfer Conference, San Diego, (1979).

16. P. Saha, "A Non-Equilibrium Heat Transfer Model for Dispersed Droplet Post-Dryout Regime," International Journal of Heat and Mass Transfer, 23, p. 481, (1980).

17. A. W. Bennett, et al., "Heat Transfer to Steam-Water Mixtures Flowing in Uniformly Heated Tubes in Which the Critical Heat Flux has been Exceeded," AERE-R-5373, (1967).

18. S. L. Soo, Fluid Dynamics of Multiphase Systems, Blaidsell Publishing Co., Waltham, MA (1967).

19. V. G. Levich, Physicochemical Hydrodynamics, Prentice-Hall, Inc., Englewood Cliffs, NJ, (1962).

20. G. B. Wallis, One Dimensional Two Phase Flow, McGraw-Hill Book Co., New York, (1969).

TABLE 1

THERMIT Conservation Equations

Conservation of Vapor Mass

$$\frac{\partial}{\partial t}(\alpha\rho_v) + \nabla\cdot(\alpha\rho_v\vec{V}_v) = \Gamma$$

Conservation of Liquid Mass

$$\frac{\partial}{\partial t}[(1-\alpha)\rho_\ell] + \nabla\cdot[(1-\alpha)\rho_\ell\vec{V}_\ell] = -\Gamma$$

Conservation of Vapor Energy

$$\frac{\partial}{\partial t}(\alpha\rho_v e_v) + \nabla\cdot(\alpha\rho_v e_v\vec{V}_v) + P\,\nabla\cdot(\alpha\vec{V}_v) + P\,\frac{\partial\alpha}{\partial t} =$$

$$= Q_{wv} + Q_i$$

Conservation of Liquid Energy

$$\frac{\partial}{\partial t}[(1-\alpha)\rho_\ell e_\ell] + \nabla\cdot[(1-\alpha)\rho_\ell e_\ell\vec{V}_\ell] + P\,\nabla\cdot[(1-\alpha)\vec{V}_\ell]$$

$$- P\,\frac{\partial\alpha}{\partial t} = Q_{w\ell} - Q_i$$

Conservation of Vapor Momentum

$$\alpha\rho_v\frac{\partial\vec{V}_v}{\partial t} + \alpha\rho_v\vec{V}_v\cdot\nabla\vec{V}_v + \alpha\nabla P = -\vec{F}_{wv} - \vec{F}_i$$

$$+ \alpha\rho_v\vec{g}$$

Conservation of Liquid Momentum

$$(1-\alpha)\rho_\ell\frac{\partial\vec{V}_\ell}{\partial t} + (1-\alpha)\rho_\ell\vec{V}_\ell\cdot\nabla\vec{V}_\ell + (1-\alpha)\nabla P = -\vec{F}_{w\ell} - \vec{F}_i$$

$$+ (1-\alpha)\rho_\ell\vec{g}$$

TABLE 2. TRAC-P1A Interfacial Exchange Models

	Bubbly Flow	Slug Flow	Annular/Annular Mist Flow
Flow Regime Criteria*	$\alpha < 0.3$ or $\alpha < 0.5$ with $G > 2700$ kg/m^{2}s	$0.3 < \alpha < 0.5$ with $G < 2000$ kg/m^{2}s	$\alpha > 0.75$
Interfacial Mass Exchange $\Gamma = -(Q_{iv}+Q_{i\ell})/i_{fg}$	Q_{iv} and $Q_{i\ell}$ same as below	Q_{iv} and $Q_{i\ell}$ same as below	Q_{iv} and $Q_{i\ell}$ same as below
Interfacial Energy Exchange $Q_{iv} = H_{iv}A_i(T_s - T_v)$ $Q_{i\ell} = H_{i\ell}A_i(T_s - T_\ell)$	$A_i = \frac{6\alpha\rho_\ell V_r^2}{We\sigma}$ We = 50 $H_{iv} = 10^4$ W/m^2 K $H_{i\ell} = \text{Max}\left\{\frac{k}{D}\left(\frac{12(T_\ell - T_s)\rho_\ell C_p}{\pi \rho_v i_{fg}}\right), \frac{k}{D}(2+0.74\ Re^{0.5})\right\}$	$A_i = \frac{3(0.92-\alpha)\rho_\ell V_r^2}{We\ \sigma} + \frac{(3\alpha-0.9)5}{D_h}$ We = 50 H_{iv} and $H_{i\ell}$ same as for bubbly flow	$A_iH_{iv} = \frac{6\alpha\rho_\ell V_r^2 E}{We\ \sigma}\left(\frac{k}{D}(2+0.74\ Re^{0.5})\right) + 5(1-E)(0.0073\ Re_v \frac{k}{D})$ $A_iH_{i\ell} = \frac{6\alpha\rho_\ell V_r^2 E}{We\ \sigma}(1500 \frac{k}{D_d} + 5(1-E)(0.0073\ Re_\ell \frac{k}{D})$ We = 2 E = Fraction of Entrained Liquid
Interfacial Momentum Exchange $F_{iv} = \frac{C_i V_r \lvert V_r \rvert}{\alpha\rho_v}$ $F_{i\ell} = \frac{C_i V_r \lvert V_r \rvert}{(1-\alpha)\rho_\ell}$	$C_i = \frac{C_b \alpha\rho_\ell}{2D_b}$ $D_b = \frac{We}{\rho_\ell V_r^2}$ We = 50 $C_b = C_b(Re)$	$C_i = \frac{\rho_\ell}{2D_b}\left(\frac{C_b(0.9-\alpha)}{2} + \frac{.44(3\alpha-0.9)}{2}\right)$ C_b and D_b same as for bubbly flow	$C_i = E\left(\frac{C_d\rho_\ell}{2D_d}\right) + (1-E)\ (0.01(1+300(1-\alpha)(1-E))$ $D_d = \frac{We\ \sigma}{\rho_\ell V_r^2}$ We = 2.0 $C_d = C_d(Re)$

* N.B. Interpolation is required between the various regimes

TABLE 3

Test Conditions for One-Dimensional

Steady-State Data

Test	Pressure Range (MPa)	Hydraulic Diameter (mm)	Mass Flux Range ($kg/m^2 \cdot s$)	Heat Flux Range (kW/m^2)	Inlet Subcooling Range (kJ/kg)
Maurer	8.3-11.0	4.1	540-1220	280-1900	150-350
Christensen	2.7-6.9	17.8	630-950	190-500	9-70
Marchaterre	1.8-4.2	11.3	600-1490	45-250	9-63

TABLE 4

Comparison of Viscous Force Coefficients

α	$\frac{36\alpha}{D_v^2}$	$\left[\frac{1. - \alpha}{\alpha D}\right]^2$
0.05	4.0×10^5	8.1×10^5
0.10	5.0×10^5	8.1×10^5
0.15	5.8×10^5	3.2×10^5
0.20	6.4×10^5	1.6×10^5
0.25	6.8×10^5	9.0×10^4
0.30	7.3×10^5	5.0×10^4

Assumptions

$D = 0.01$ m

$D_v = 2(\alpha / \frac{4\pi}{3} N)^{1/3}$

with $N = 10^7$ bubbles/m^3

TABLE 5

Comparison of Inertial Force Coefficients

α	$0.01(1 + 75(1 - \alpha))\sqrt{\alpha}$	$\frac{1 - \alpha}{2\alpha}$
0.4	0.29	0.75
0.5	0.27	0.50
0.6	0.24	0.33
0.7	0.20	0.21
0.8	0.14	0.13
0.9	0.08	0.06

TABLE 6

THERMIT Interfacial Exchange Models

	Pre-CHF Regime	Post-CHF Regime
Interfacial Mass Exchange	$\Gamma = \begin{cases} 0 & T_\ell < T_d \\ \frac{T_\ell - T_d}{T_s - T_d}\,\Gamma_e + A_i H_i (T_\ell - T_v)/i_{fg} & T_d < T_\ell < T_s \\ \Gamma_e & T_\ell \geq T_s \end{cases}$ Eq. (10)	$\Gamma = 6300 \left(1 - \frac{P}{P_{cr}}\right)^2 \left(\frac{\rho_v V_v^2 D}{\sigma}\right)^{1/2} \frac{k_v (T_v - T_s)}{D^2 i_{fg}} (1-\alpha)$ Eq. (16)
Interfacial Energy Exchange	$Q_i = H_{iv}(T_s - T_v) + \Gamma i_g$ Eq. (19)	$Q_i = \Gamma i_f - H_{i\ell}(T_s - T_\ell)$ Eq. (20)
Interfacial Momentum Exchange	$F_i = \left(\frac{1-\alpha}{\alpha D}\right)^2 \mu_\ell V_r + \left(\frac{1-\alpha}{\alpha D}\right) \frac{\rho_v \lvert V_r \rvert V_r}{2}$ Eq. (27)	Same as in Pre-CHF

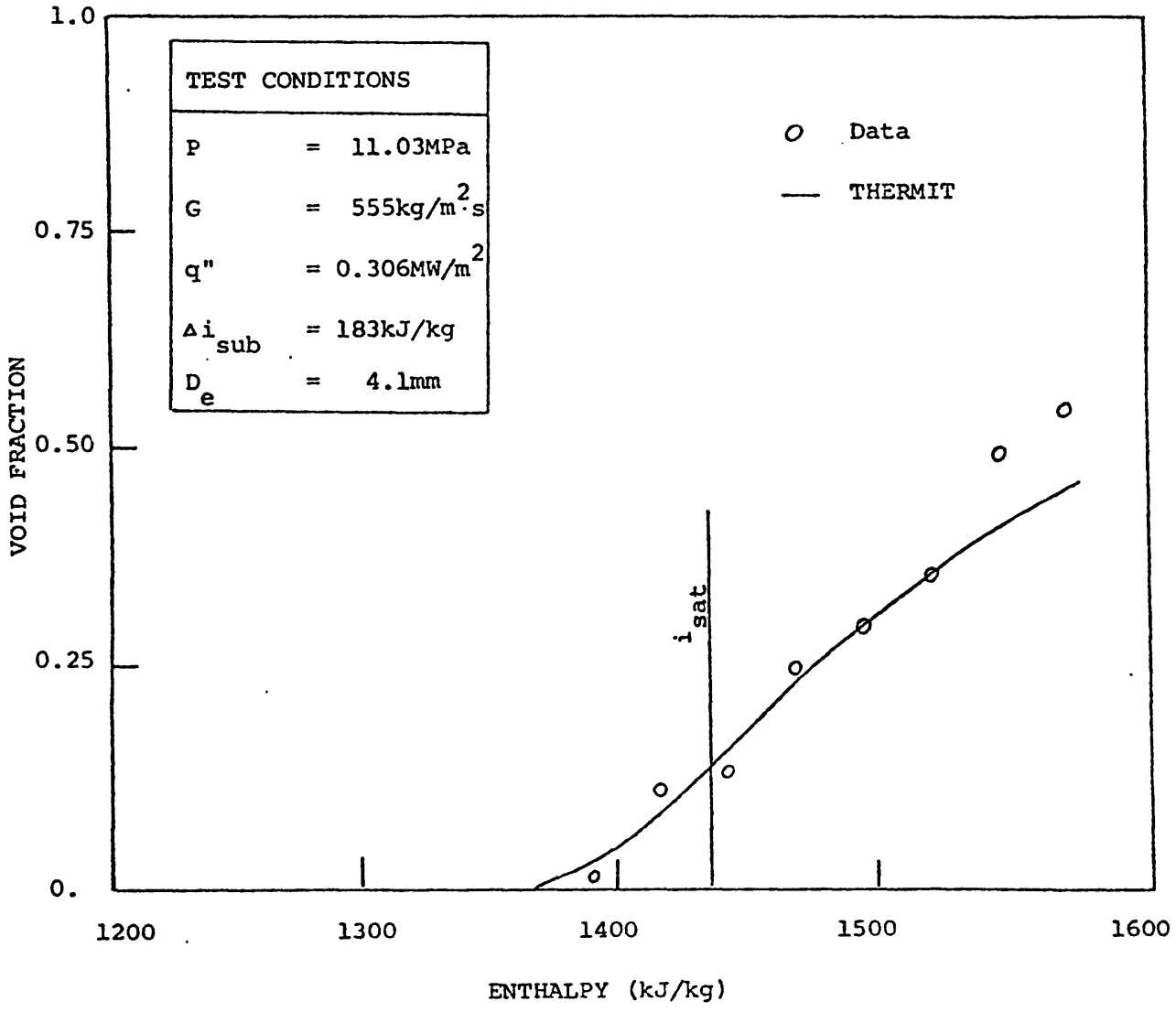

Figure 1: Void Fraction versus Enthalpy for Maurer Case 214-9-3

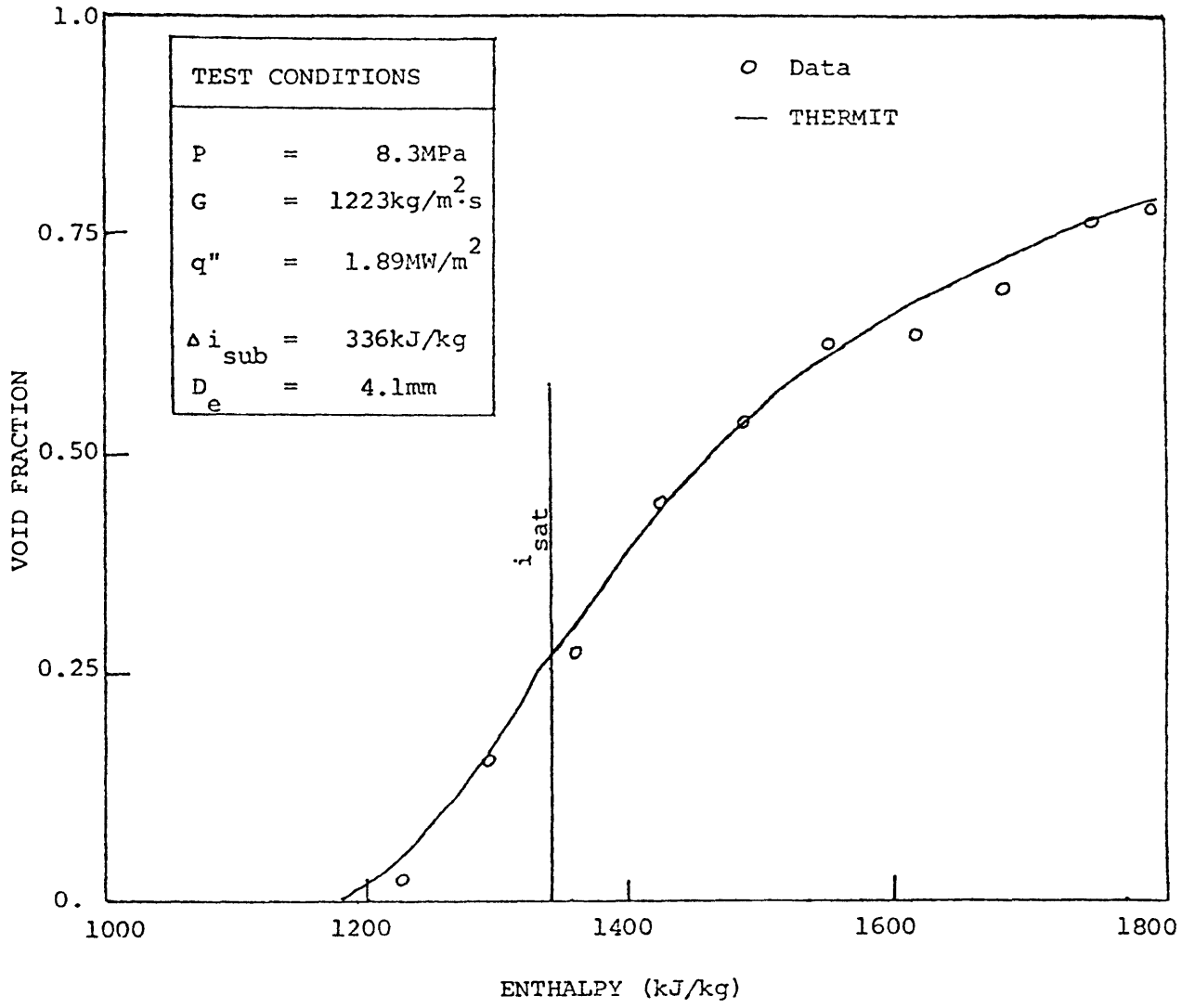

Figure 2: Void Fraction versus Enthalpy - Maurer Case 214-3-5

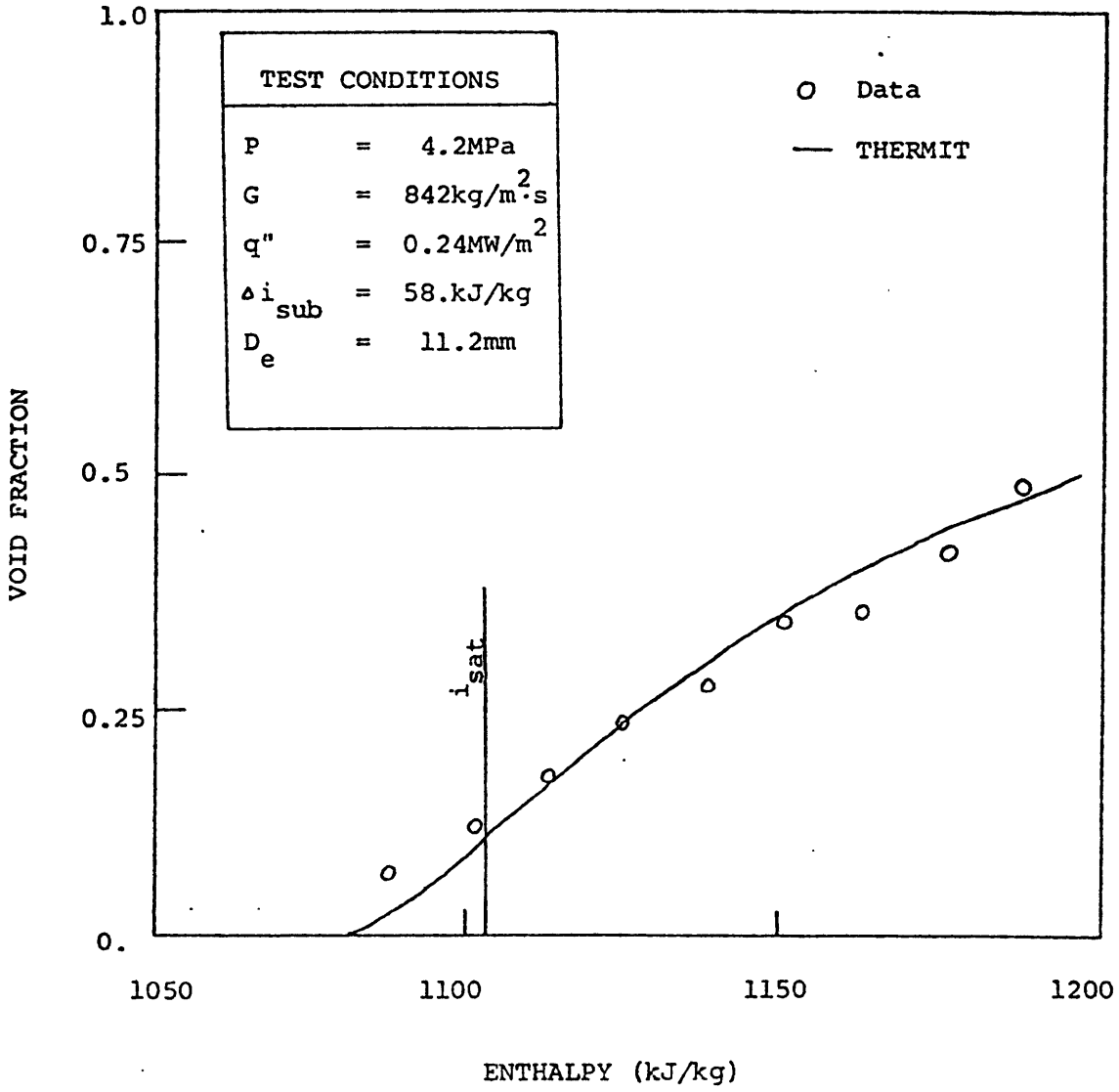

Figure 3: Void Fraction versus Enthalpy for Marchaterre Case 168

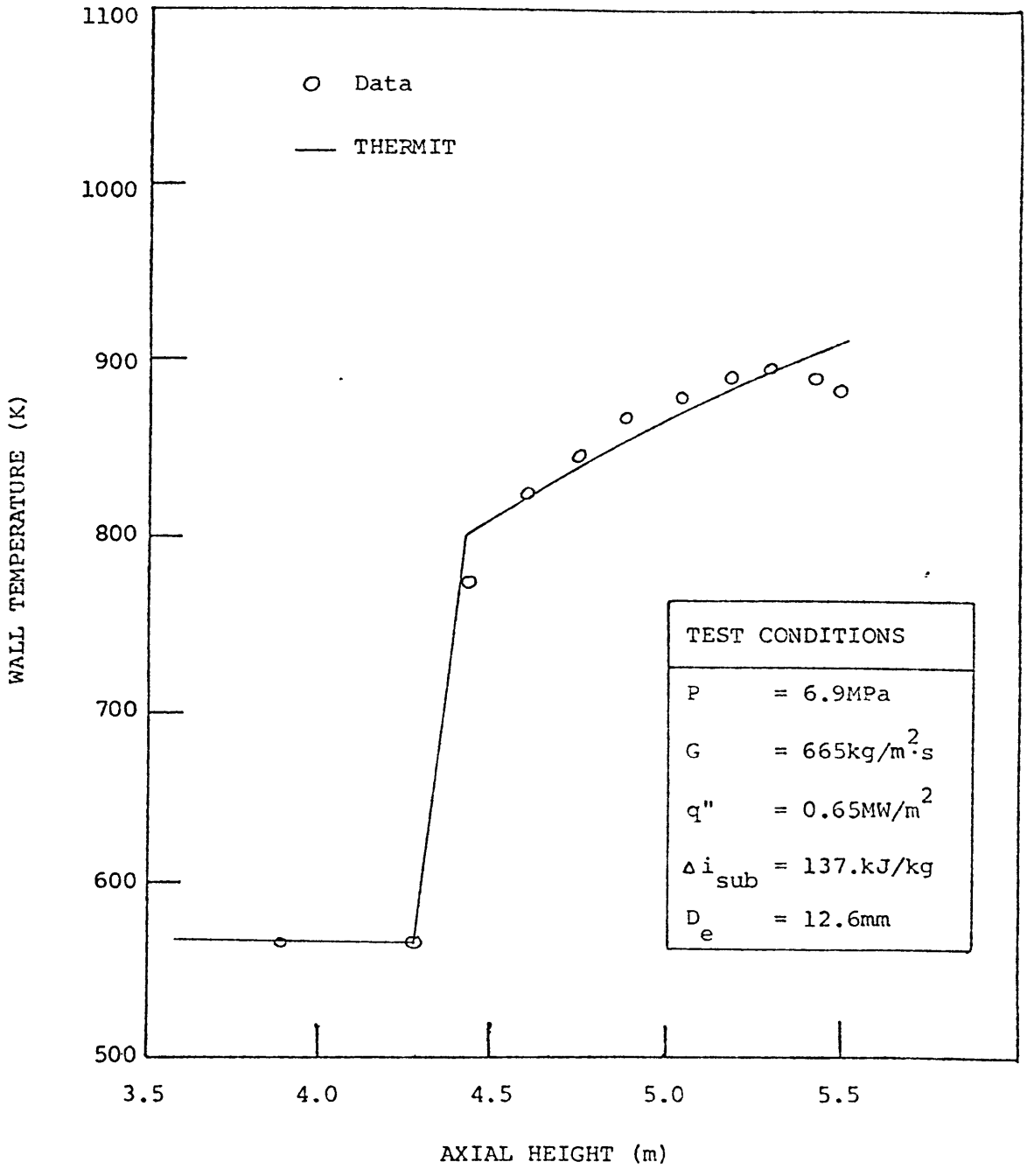

Figure 4: Wall Temperature Comparisons for Bennett Case 5332 (Length = 5.56m)

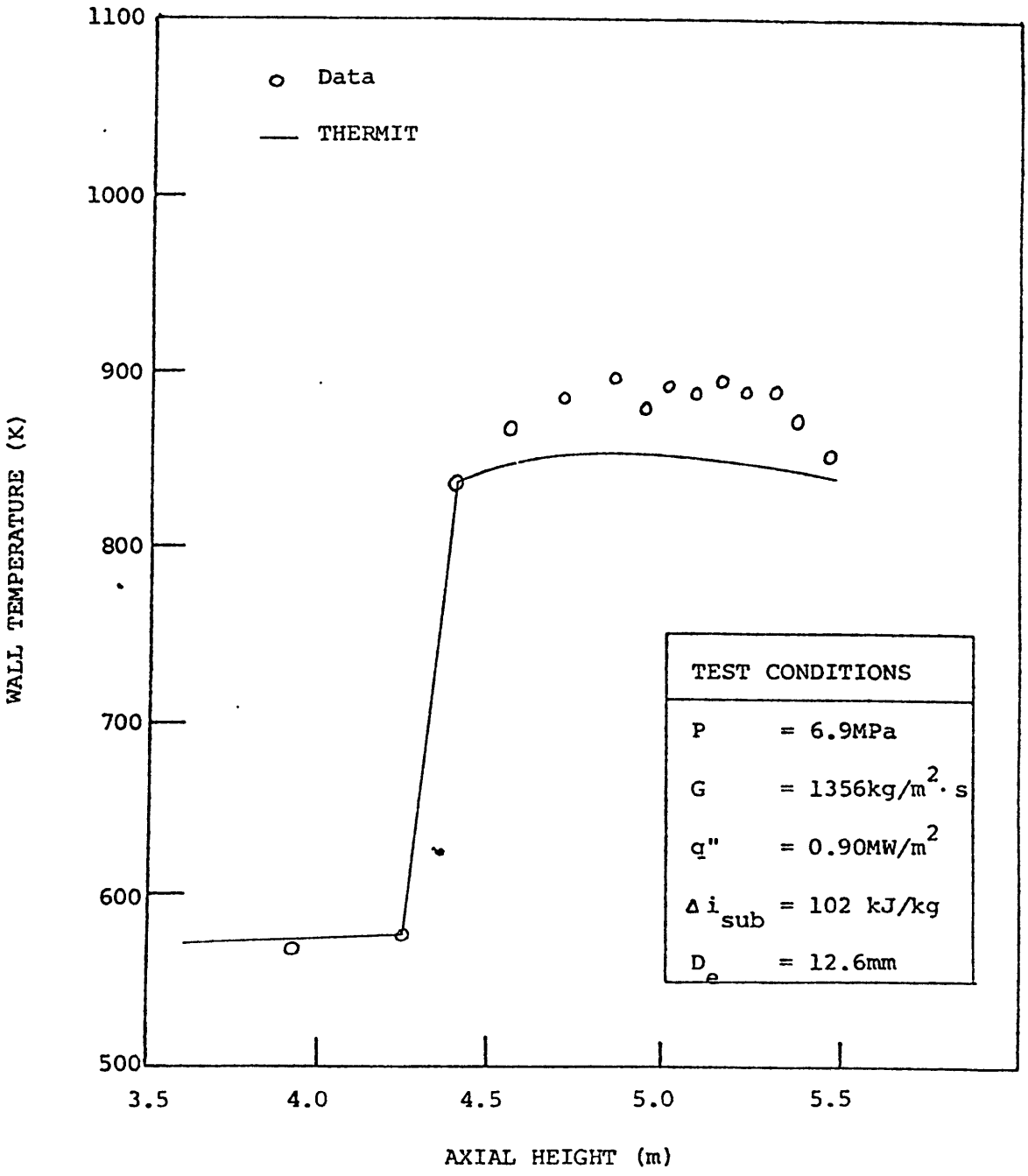

Figure 5: Wall Temperature Comparisons for Bennett Case 5253

(Length = 5.56m)

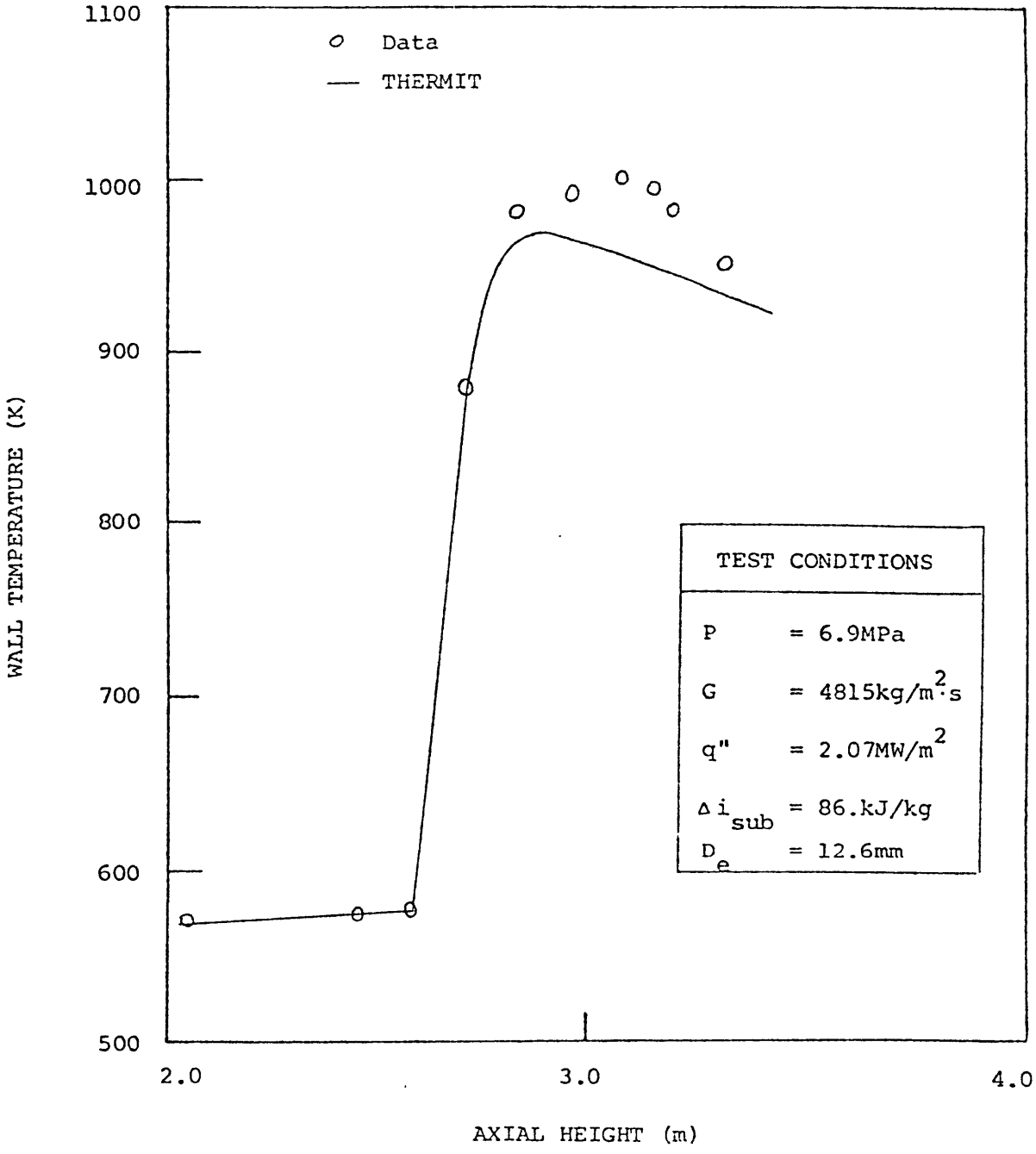

Figure 6: Wall Temperature Comparisons for Bennett Case 5442 (Length = 3.66m)

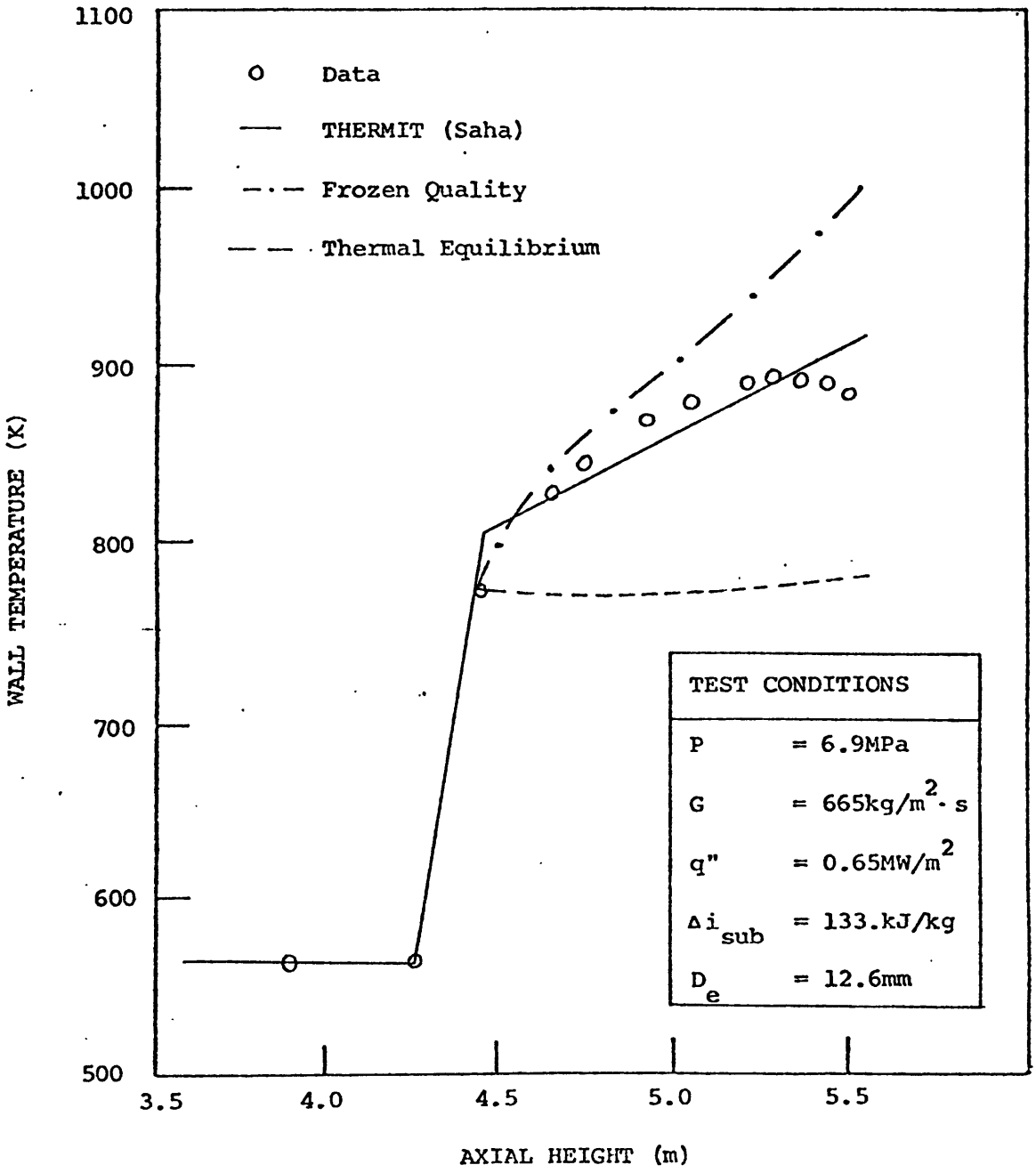

Figure 7: Comparison of Wall Temperature Predictions Using Various Γ Models for Bennett Case 5332

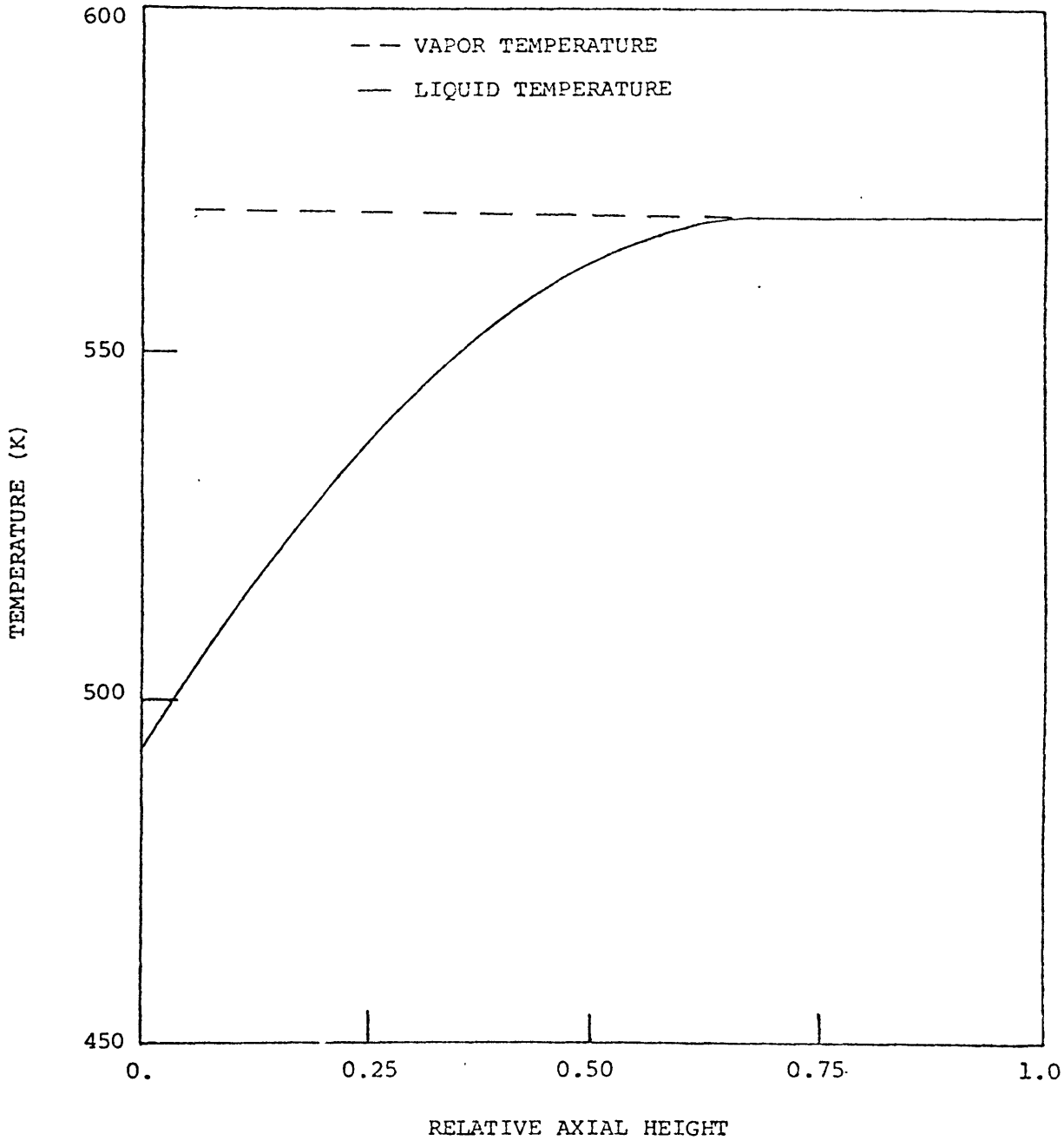

Figure 8: Predicted Liquid and Vapor Temperatures for Maurer Case 214-3-5

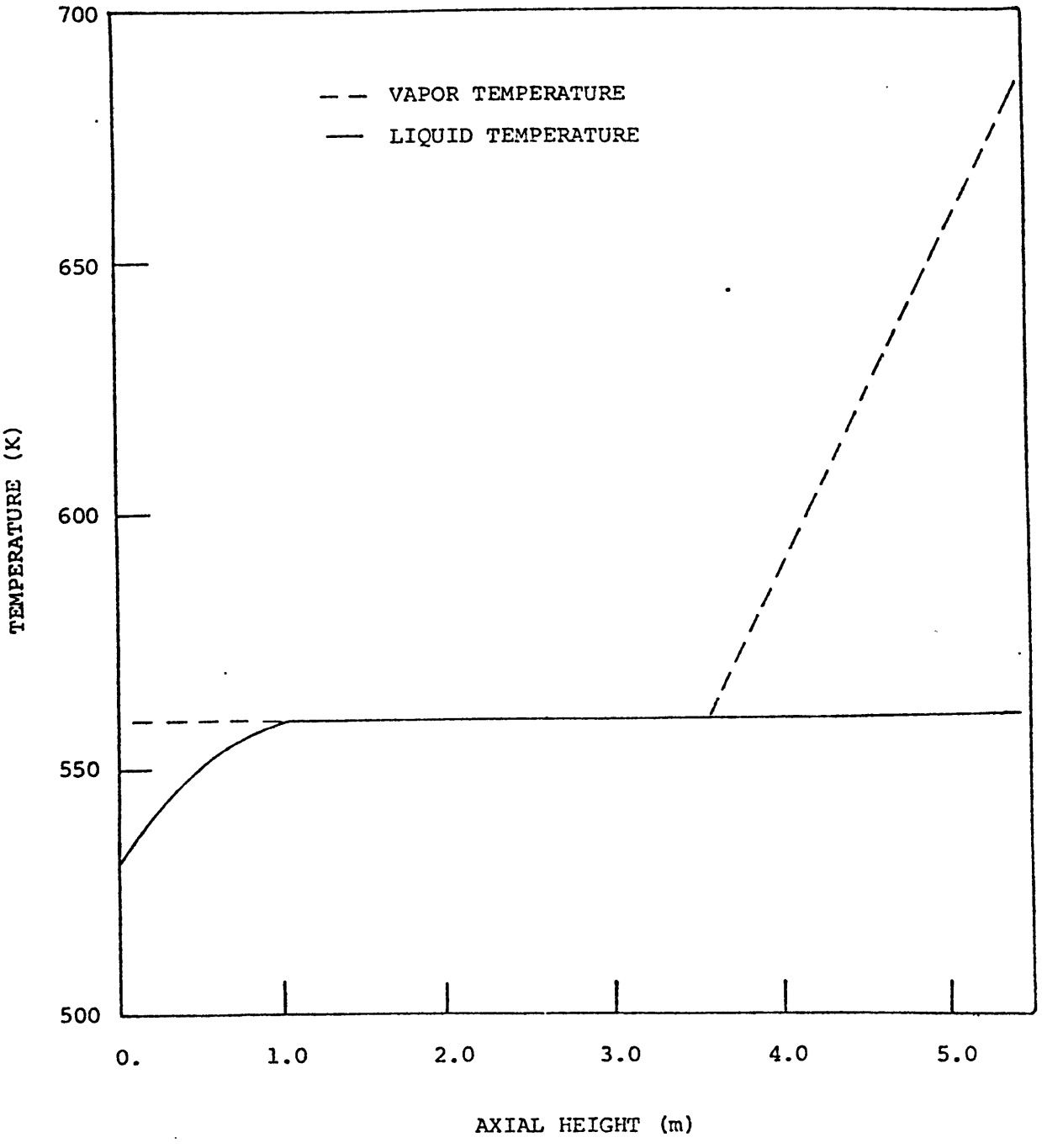

Figure 9: Predicted Liquid and Vapor Temperatures for Bennett Case 5336

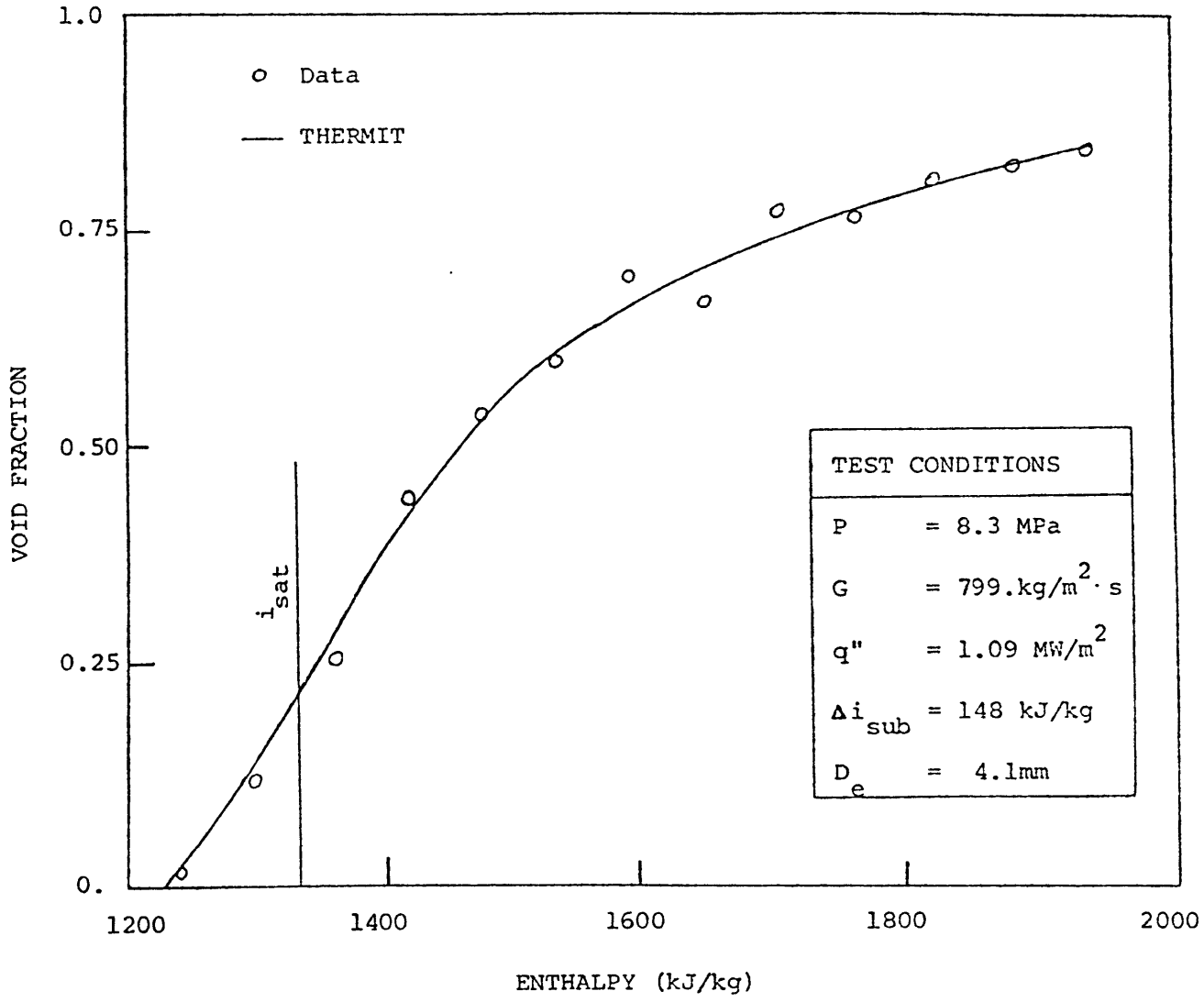

Figure 10: Void Fraction versus Enthalpy for Maurer Case 214-3-4

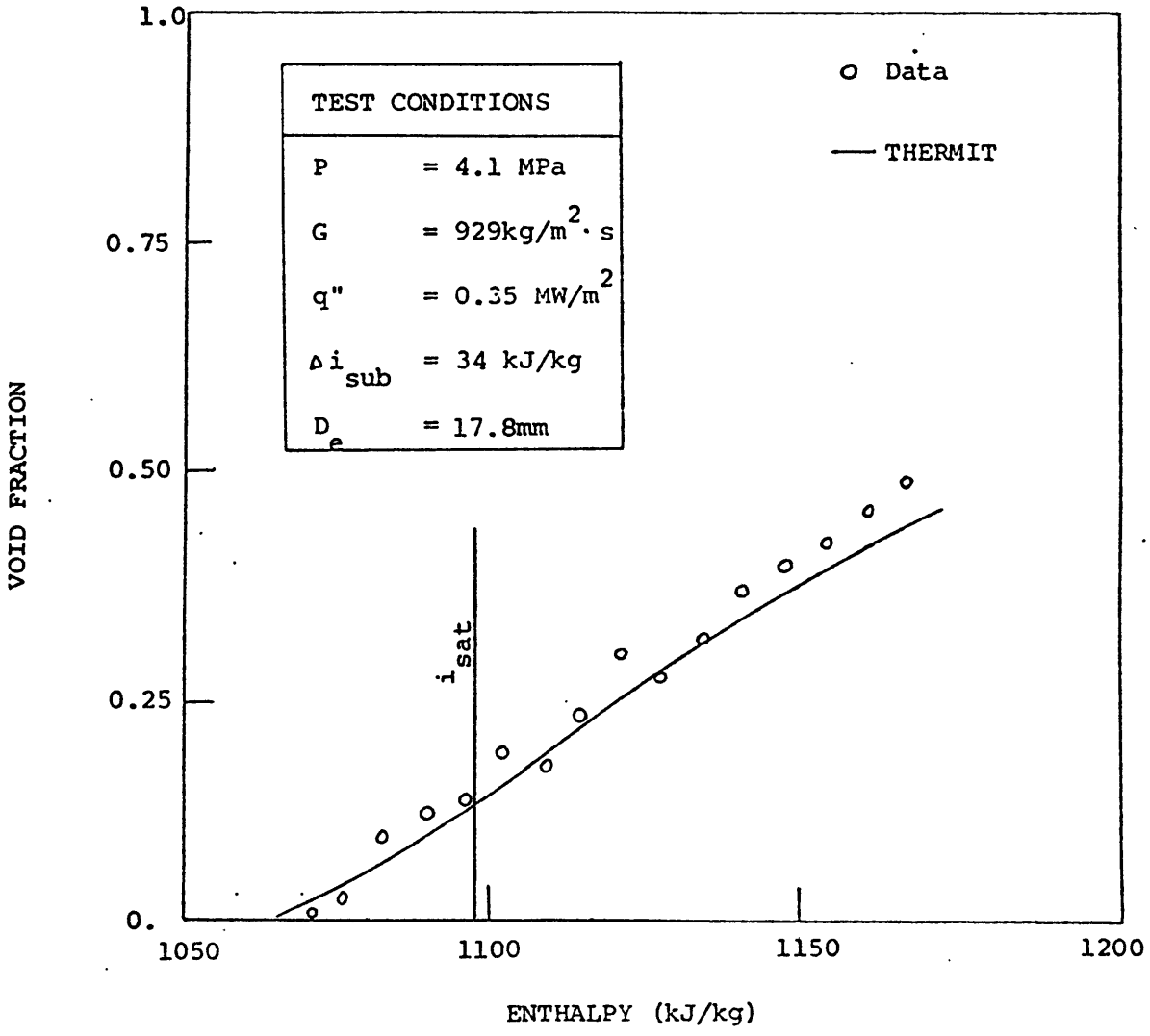

Figure 11: Void Fraction versus Enthalpy for Christensen Case 12

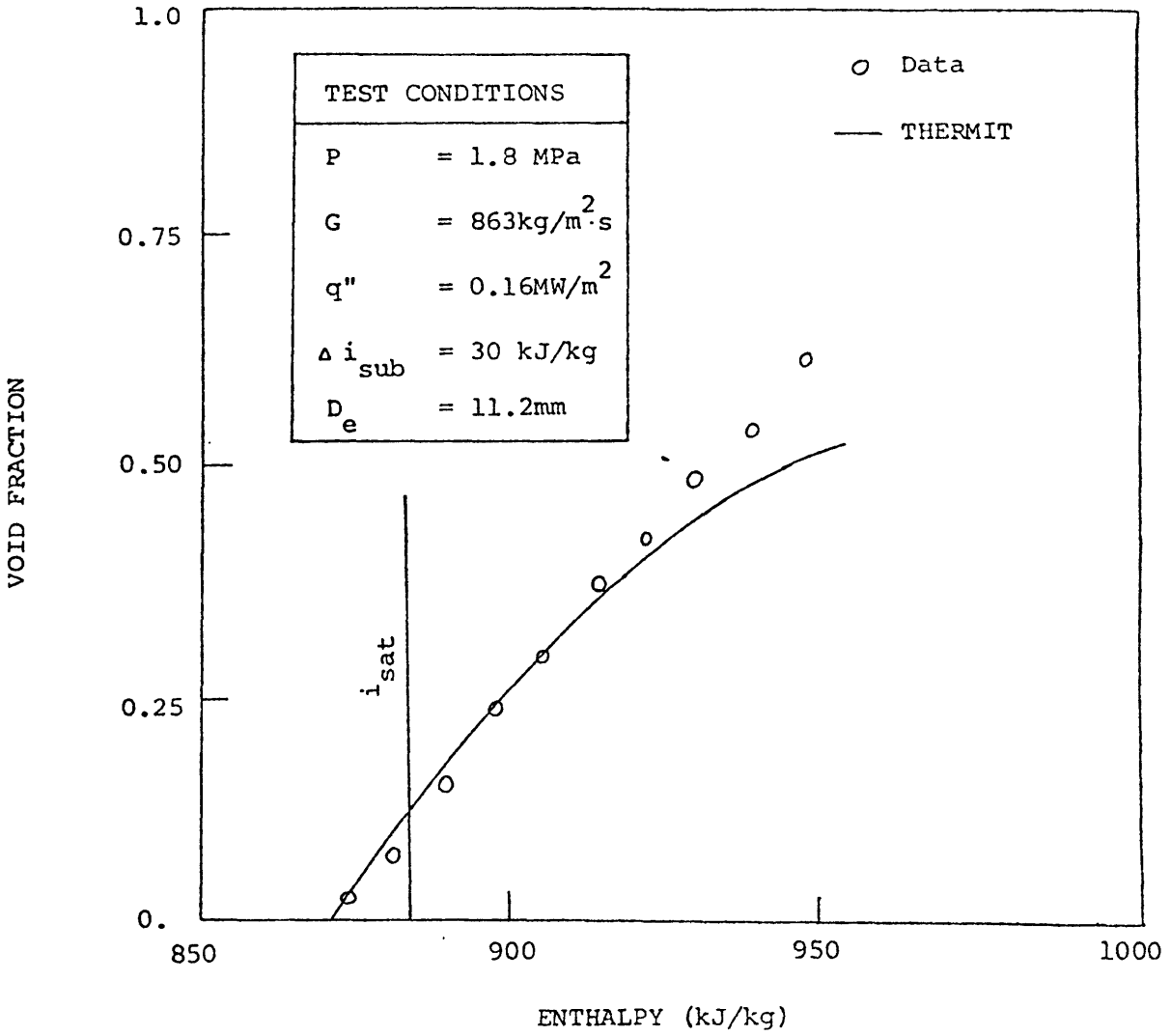

Figure 12: Void Fraction versus Enthalpy for Marchaterre Case 185